Mesoporous TiO2 Core–Shell Spheres Composed of Nanocrystals with Exposed High-Energy Facets: Facile Synthesis and Formation Mechanism

ARTICLE *in* LANGMUIR · JUNE 2011

Impact Factor: 4.46 · DOI: 10.1021/la201547g · Source: PubMed

8 AUTHORS, INCLUDING:

Liu Baoshun
Wuhan University of Technology
60 PUBLICATIONS **934** CITATIONS
SEE PROFILE

Munetoshi Sakai
Science University of Tokyo, Yamaguchi
76 PUBLICATIONS **737** CITATIONS
SEE PROFILE

Tsuyoshi Ochiai
Kanagawa Academy of Science and Technol…
72 PUBLICATIONS **869** CITATIONS
SEE PROFILE

Katsuhiko Takagi
Nagoya University
113 PUBLICATIONS **2,249** CITATIONS
SEE PROFILE

Langmuir

ARTICLE

pubs.acs.org/Langmuir

Mesoporous TiO_2 Core−Shell Spheres Composed of Nanocrystals with Exposed High-Energy Facets: Facile Synthesis and Formation Mechanism

Baoshun Liu,[†] Kazuya Nakata,*[,†,‡,§] Munetoshi Sakai,[†,‡] Hidenori Saito,[‡] Tsuyoshi Ochiai,[†,§] Taketoshi Murakami,[†] Katsuhiko Takagi,[‡] and Akira Fujishima*[,†,‡,§]

[†]Photocatalyst Group, Kanagawa Academy of Science and Technology, KSP Building East 412, 3-2-1 Sakado, Takatsu-ku, Kawasaki, Kanagawa 213-0012, Japan

[‡]Organic Solar Cell Assessment Project, Kanagawa Academy of Science and Technology, KSP Building East 308, 3-2-1 Sakado, Takatsu-ku, Kawasaki, Kanagawa 213-0012, Japan

[§]Research Institute for Science and Technology, Energy and Environment Photocatalyst Research Division, Tokyo University of Science, 1-3 Kagurazaka, Shinjuku-ku, Tokyo 162-8601, Japan

ABSTRACT: A facile new method that combines electrospray and hydrothermal treatment is used to prepare mesoporous core−shell TiO_2 spheres with high specific surface areas and high pore volumes. Interestingly, the resulting TiO_2 spheres are composed of anatase TiO_2 nanocrystals with exposed step-like {001} and smooth {010} facets. The percentage of exposed {001} facets can be adjusted by changing the experimental parameters used in the electrospray and hydrothermal treatment processes, such as the contents of poly(*N*-vinyl-2-pyrrolidone) and acetic acid. The combination of high specific surface area (>100 $m^2\ g^{-1}$), high pore volume (>0.30 $cm^3\ g^{-1}$), useful pore size (10−15 nm), spherical core−shell structure, and exposed high energy facets makes these TiO_2 spheres an important candidate for use in many photoelectrochemical applications. The formation mechanism of the mesoporous TiO_2 spheres is also studied. The great advantage of this method is that interesting and complicated mesoporous superstructures can be prepared using electrospray technology.

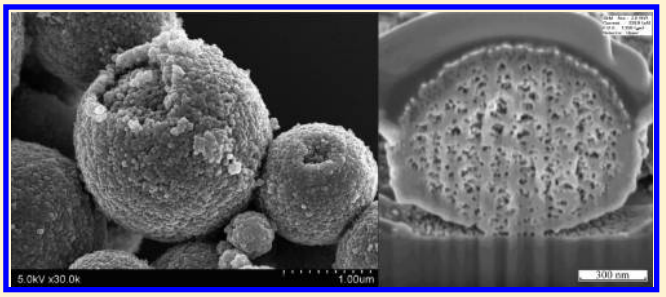

INTRODUCTION

Mesoporous TiO_2 materials currently attract significant attention for application in the heterogeneous photocatalysis,[1−3] dye-sensitized solar cells (DSSCs),[4−6] lithium ion batteries,[7,8] and electrochromic displays.[9] Mesoporous TiO_2 materials of different structure and morphology including films,[10] arrays,[11] fibers,[12] mesocrystals,[13] spheres,[14−17] and tubes[18,19] have been produced. Mesoporous TiO_2 spheres are one of the most interesting materials because of their structure and properties. Such spheres have been prepared by methods such as hydrolysis of glycolate titanium spheres,[14] hydrothermal treatment of sol−gel titania spheres,[6] and a template-free hydrothermal process.[20] These spheres usually possess a high specific surface area, high pore volume, and pore size that make them good candidates for use in photocatalysis, DSSCs,[21] and other fields.[15,20] Importantly, properties of mesoporous TiO_2 spheres including light scattering[6,21] and multireflection[20] can improve their photocatalytic activity and the performance of DSSCs.

Anatase TiO_2 crystals with exposed high-energy facets, including {001} and {010} facets, have attracted significant attention because of their high chemical activity.[22−34] TiO_2 spheres that are composed of such crystals should exhibit interesting properties because high chemical activity would be integrated into mesoporous TiO_2 spheres. Recently, a method involving fluoride-mediated self-transformation was used to prepare hollow TiO_2 spheres composed of TiO_2 crystals with exposed {001} facets.[35,36] However, these crystals were too large to obtain a high specific surface area and suitable pore structure. Although much smaller nanocrystals (∼13 nm) with exposed high energy facets can be obtained using a surfactant-capping solvothermal method,[37] to prepare mesoporous spheres consisting of TiO_2 nanocrystals with exposed high energy facets remains a challenge.

Here, we report a facile method that combines electrospray and hydrothermal post-treatment to prepare mesoporous core−shell spheres composed of very small TiO_2 nanocrystals with exposed step-like {001} and {010} facets. Electrospray and electrospinning techniques are used to prepare the materials consisting of fibers, tubes, and spheres.[38−44] More complicated materials, such as spheres composed of three phases[43,44] or multiple components[40] and multichannel tubes,[41,42] can be obtained using cojetting methods. Electrospray and electrospinning processes can be used to prepare interesting materials with

Received: April 27, 2011
Revised: May 15, 2011
Published: June 07, 2011

Table 1. Properties of Electrosprayed TiO_2 Spheres and the Same Spheres after Annealing

sample	S_{BET} ($m^2\ g^{-1}$)[a]	V_p ($cm^3\ g^{-1}$)[b]	D_p (nm)[c]	R (%)
electrosprayed[d]	60	0.54	60	
after annealing	32	0.07	13	20

[a] Specific surface area. [b] Pore volume accumulated from 2 to 100 nm. [c] Average pore size. [d] Electrosprayed TiO_2 spheres were washed with a mixture of water and ethanol for 20 min.

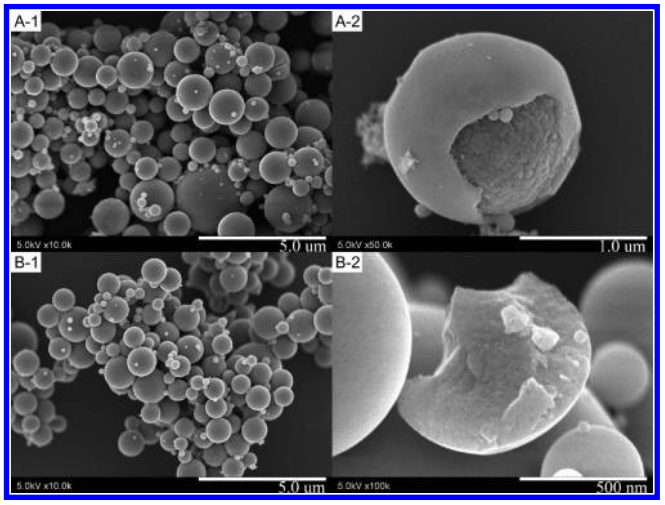

Figure 1. FE-SEM images of the (A) electrosprayed TiO_2 spheres and (B) TiO_2 spheres after annealing at 500 °C for 2 h.

different structures. Annealing is usually used to induce crystallization and remove organic substances from electrosprayed or -spun materials, but this procedure always causes the materials to shrink, reduces their specific surface area, and destroys pore structures. Herein, we show that the as-sprayed TiO_2 spheres subjected to hydrothermal treatment possess a completely different structure to annealed spheres. Using our method, mesoporous core−shell superstructures with high specific surface area and high pore volume are produced. Interestingly, these TiO_2 spheres are composed of tiny TiO_2 crystals with exposed step-like {001} and flat {010} facets. The percentage of exposed {001} facets can be adjusted by changing the amounts of poly(*N*-vinyl-2-pyrrolidone) (PVP) and acetic acid used in the procedure. The high specific surface area, mesoporous core−shell structure, and exposed high-energy facets make such TiO_2 materials excellent candidates for application in energy conversion and environmental cleanup.

EXPERIMENTAL SECTION

Electrospray process. First, PVP K30 (M_w = 25 000, 0.1−0.7 g) was dissolved in a mixture of ethanol (2.5 mL) and acetic acid (3.8 mL) with stirring. After 10 min, titanium butoxide (TBT, 7.0 mL) was added, and then the mixture was stirred continuously for 1 h to obtain a uniform pale yellow PVP-Ti sol. The PVP−TBT sol was loaded in a syringe pump and then pumped through a small metal nozzle (23 G needle with ϕ_{in} = 0.33 mm) onto a large aluminum target placed about 35 cm away at a rate of 1.0 mL h^{-1}. A voltage of 35 kV was applied between the metal needle and aluminum target to maintain a stable Taylor cone. The electrospray setup was very stable and can operate for many hours.

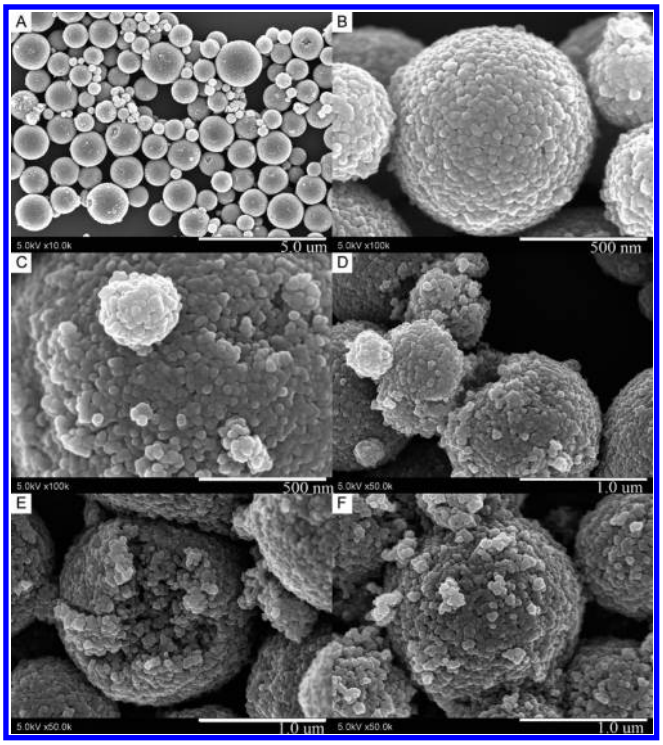

Figure 2. FE-SEM images of TiO_2 spheres after hydrothermal treatment in an ethanol/water mixture containing (A, B) 0, (C) 0.5, (D) 2.0, (E) 3.0, and (F) 4.0 mL of acetic acid.

After about 3−4 h, the materials on the target were collected and dried in air for at least 6 h.

Hydrothermal Process: Effect of Acetic Acid. The material obtained from electrospray (0.2 g) was dispersed in a solution of deionized water (10 mL) and ethanol (20 mL) with stirring. After 10 min, acetic acid (0, 0.5, 1.0, 2.0, 3.0, or 4.0 mL) was added; the mixture was placed in a 50 mL autoclave and then treated hydrothermally at 160 °C for 24 h. After hydrothermal treatment, the reaction solution was cleaned with ethanol and centrifuged at least three times. The TiO_2 materials were dried at about 50 °C to obtain a TiO_2 powder suitable for characterization.

Hydrothermal Process: Effect of Hydrothermal Treatment Time. The material obtained from electrospray (0.2 g) was dispersed in a solution of deionized water (10 mL) and ethanol (20 mL) with stirring. After 10 min, acetic acid (2.0 mL) was added, and then the solution was placed in an autoclave for hydrothermal treatment at 160 °C for 5, 10, 20, or 24 h. The procedure followed to clean and dry the material was the same as that described in the above section.

Hydrothermal Process: Effect of PVP Content in the Materials Obtained after Electrospray. The materials obtained from electrospray (0.2 g) PVP−TBT sols containing different amounts of PVP (0.1−0.7 g) were dispersed in a solution containing water (10 mL) and ethanol (20 mL). After stirring for 10 min, acetic acid (2.0 mL) was added, and then the mixtures were placed in autoclaves for hydrothermal treatment at 160 °C for 24 h. The procedure followed to clean and dry the material was the same as that described above.

Characterization. Powder X-ray diffraction (RINT1500, Rigaku, Japan) was used to determine the crystalline phase and calculate the crystal size in the mesoporous polydisperse TiO_2 spheres. The morphology of the samples was observed using a high-resolution field emission scanning electron microscope (FE-SEM, Hitachi S-4800, Hitachi, Tokyo, Japan). Transmission electron microscope (TEM) images of the mesoporous TiO_2 spheres were obtained using a

dx.doi.org/10.1021/la201547g |*Langmuir* 2011, 27, 8500–8508

FE-TEM (EM002BF, Topcon, Tokyo, Japan) operating at 200 kV. Nitrogen adsorption isotherms were measured at −196 °C using a Micromeritics system (Gemini V, Shimadzu, Japan). Prior to measurement, the samples were first degassed at 200 °C on a vacuum line for 1 h. The multipoint Brunauer−Emmett−Teller (BET) method was used to calculate the surface area from the adsorption data in the range of P/P_0 from 0.05 to 0.2. The pore size distributions of the samples were derived from the adsorption data using the Barett−Joyner−Halenda (BJH) model. Calculated pore volumes ranged from 2 to 100 nm. The cross-sectional morphology of the mesoporous TiO_2 spheres was observed using focused ion beam (FIB)-SEM-Ar ion milling equipment (XVision 200TB, Seiko, Chiba, Japan).

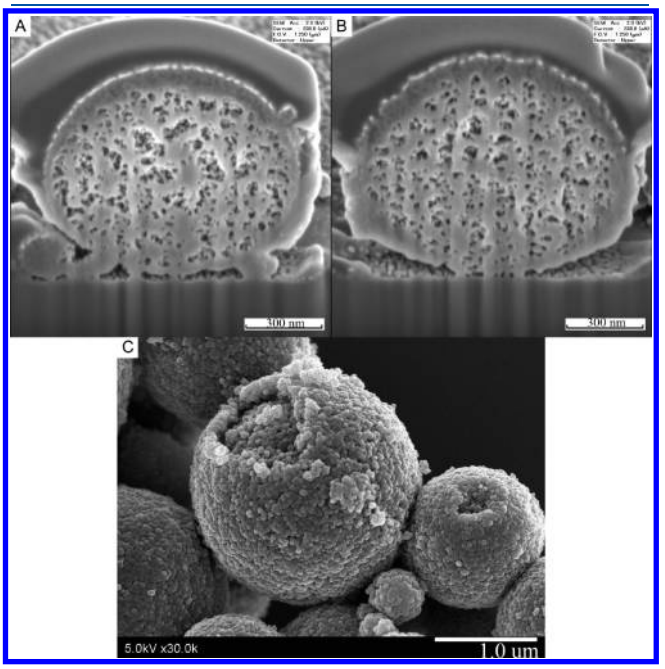

Figure 3. Cross-sectional SEM images of cut TiO_2 spheres obtained after hydrothermal treatment with (A) 0 and (B) 2.0 mL of acetic acid; (C) shows an FE-SEM image of the sample obtained after hydrothermal treatment with 2.0 mL of acetic acid.

RESULTS AND DISCUSSION

Electrosprayed TiO_2 Spheres and the Effect of Annealing. Field-emission scanning electron microscope (FE-SEM) images of the electrosprayed and annealed TiO_2 spheres are shown in Figure 1. The electrosprayed TiO_2 spheres are polydisperse with diameters ranging from several tens of nanometers to several micrometers. The size of the electrosprayed spheres can readily be adjusted by changing the flow rate during electrospray. Smaller TiO_2 spheres are obtained when the flow rate is decreased to 0.5 mL h^{-1}. The electrosprayed TiO_2 spheres possess a smooth, dense surface, but the inner structure contains many large pores, as shown in Figure 1A-2. BET analysis showed the presence of pores with a diameter of 60 nm in the spheres (Table 1). This observation reveals that the electrosprayed TiO_2 spheres possess an interesting core (porous)−shell (smooth) structure. The spheres show obvious shrinkage after annealing because of crystallization of amorphous TiO_2, the removal of organic substances, and the collapse of large pores, as shown in Figure 1B-1. An FE-SEM image of a broken TiO_2 sphere (Figure 1B-2) shows that annealing increases the density of the

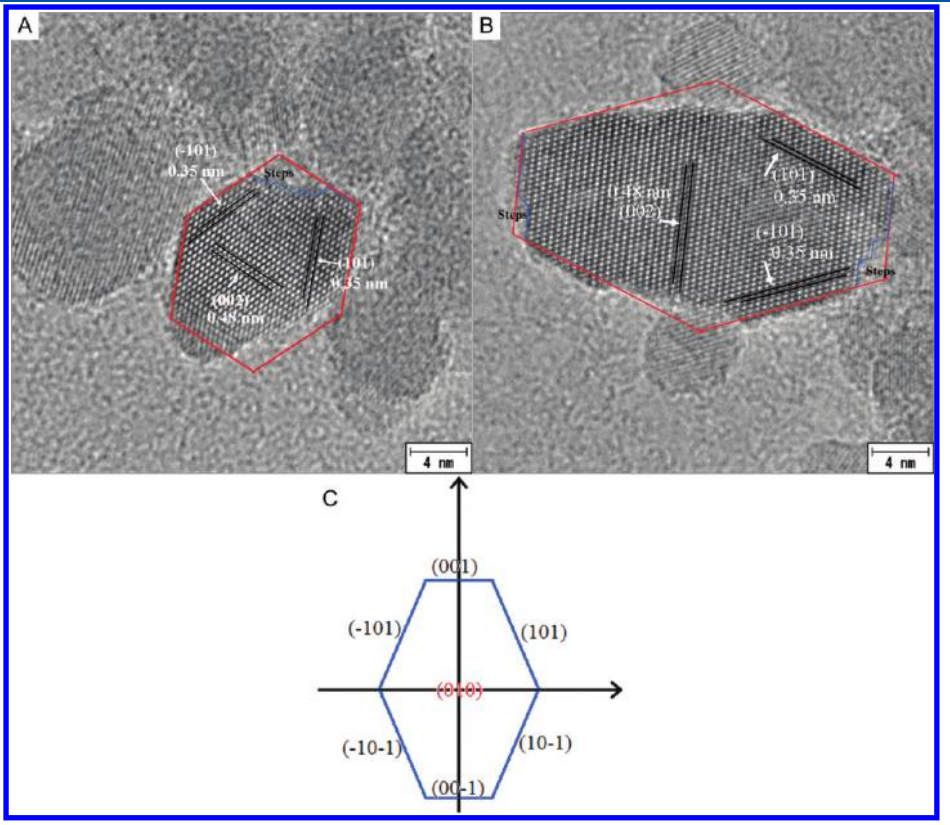

Figure 4. High-magnification TEM images of the TiO_2 nanocrystals in the TiO_2 spheres after hydrothermal treatment with (A) 0 and (B) 2.0 mL of acetic acid. (C) Schematic illustration of crystal facets for the TiO_2 nanocrystals.

dx.doi.org/10.1021/la201547g |*Langmuir* 2011, 27, 8500–8508

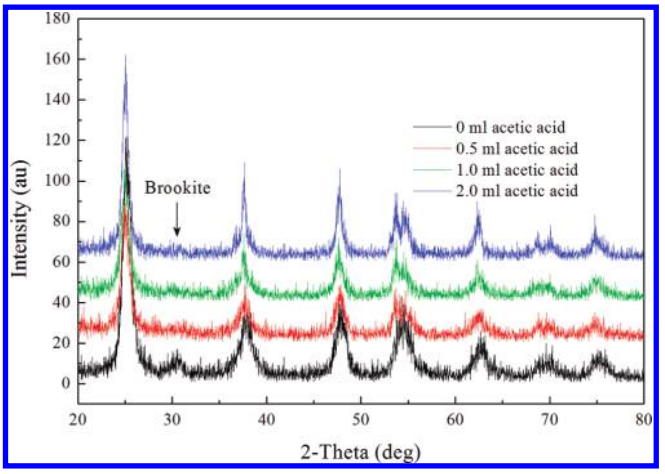

Figure 5. XRD patterns of TiO_2 spheres obtained after hydrothermal treatment with different amounts of acetic acid.

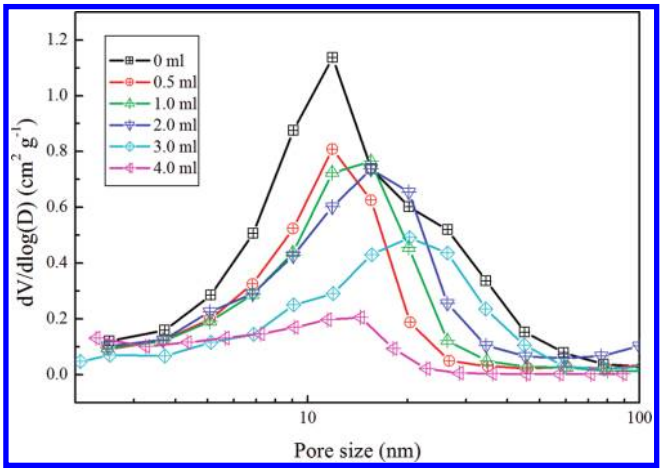

Figure 6. Pore size distributions of the mesoporous TiO_2 spheres obtained after hydrothermal treatment with different amounts of acetic acid.

Table 2. Properties of Mesoporous TiO_2 Spheres after Hydrothermal Post-treatment in Acetic Acid Solution

amount of acetic acid (mL)	S_{BET} (m^2 g^{-1})	V_p (cm^3 g^{-1})	percent of pores (%)	D_p (nm)
0	198	0.67	72	12, 26
0.5	134	0.38	59	12
1.0	137	0.40	61	15.5
2.0	135	0.36	58	15.4
3.0	105	0.32	55	20
4.0	108	0.31	54	14

Table 3. Properties of Mesoporous TiO_2 Spheres after Hydrothermal Treatment for Different Periods

time (h)	S_{BET} (m^2 g^{-1})	V_p (cm^3 g^{-1})	D_p (nm)	percentage of pores (%)
0[a]	60	0.54	60	
5	188	0.40	12	61
15	155	0.39	12	60
20	148	0.38	15	59
24	135	0.36	15	58

[a] Electrosprayed TiO_2 spheres obtained after washing with a mixture of water and ethanol for 20 min.

porous inner structure of the electrosprayed TiO_2 spheres, finally resulting in the amalgamation of the shell and core structures. This finding is supported by BET analysis (Table 1), which shows that the specific surface area and pore volume obviously decrease after annealing.

Effect of Acetic Acid on Hydrothermal Treatment. FE-SEM images of the TiO_2 spheres obtained after hydrothermal treatment in a solution of water, ethanol, and acetic acid are shown in Figure 2. Compared with the electrosprayed TiO_2 spheres, the surfaces of the samples after hydrothermal treatment are composed of numerous nanoparticles and become very rough. Figure 2A,B shows FE-SEM images of the sample obtained after hydrothermal treatment without acetic acid. In this sample, nanoparticles are tightly compacted to form a dense surface. The addition of acetic acid during hydrothermal treatment cause the TiO_2 spheres to become less dense, and some spheres tended to break into smaller particles if more than 2.0 mL of acetic acid was added (Figure 2D). Moreover, small pores with diameters of 10−20 nm can be seen on the surface of the spheres, indicating mesoporous structures. Figure 2E shows an FE-SEM image of the sample obtained after hydrothermal treatment with addition of 3.0 mL of acetic acid. A broken sphere was chosen to allow the inner structure to be observed. It can be seen that some large pores (about 50 nm) are present, unlike the surface structure.

The inner structure of the samples after hydrothermal treatment was also studied using a focused ion beam (FIB)-SEM-Ar ion milling technique. In this technique, a selected sphere is cut in half and then observed using a SEM probe attached to the FIB

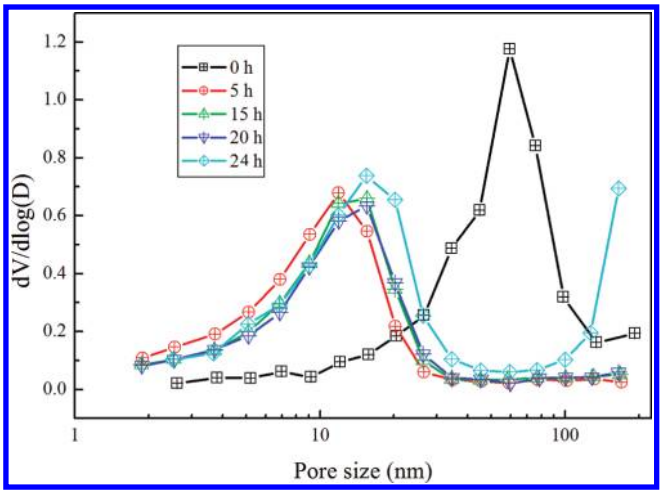

Figure 7. Pore size distributions of the mesoporous TiO_2 spheres obtained after hydrothermal treatment for different periods.

equipment. Parts A and B of Figure 3 show cross-sectional images of the spheres after hydrothermal treatment without and with 2.0 mL of acetic acid, respectively. Interestingly, the TiO_2 spheres show a core−shell structure after hydrothermal treatment without acetic acid. The shells are dense and contain many nanosized pores. The inner core also contains some larger pores, indicating

dx.doi.org/10.1021/la201547g |*Langmuir* 2011, 27, 8500–8508

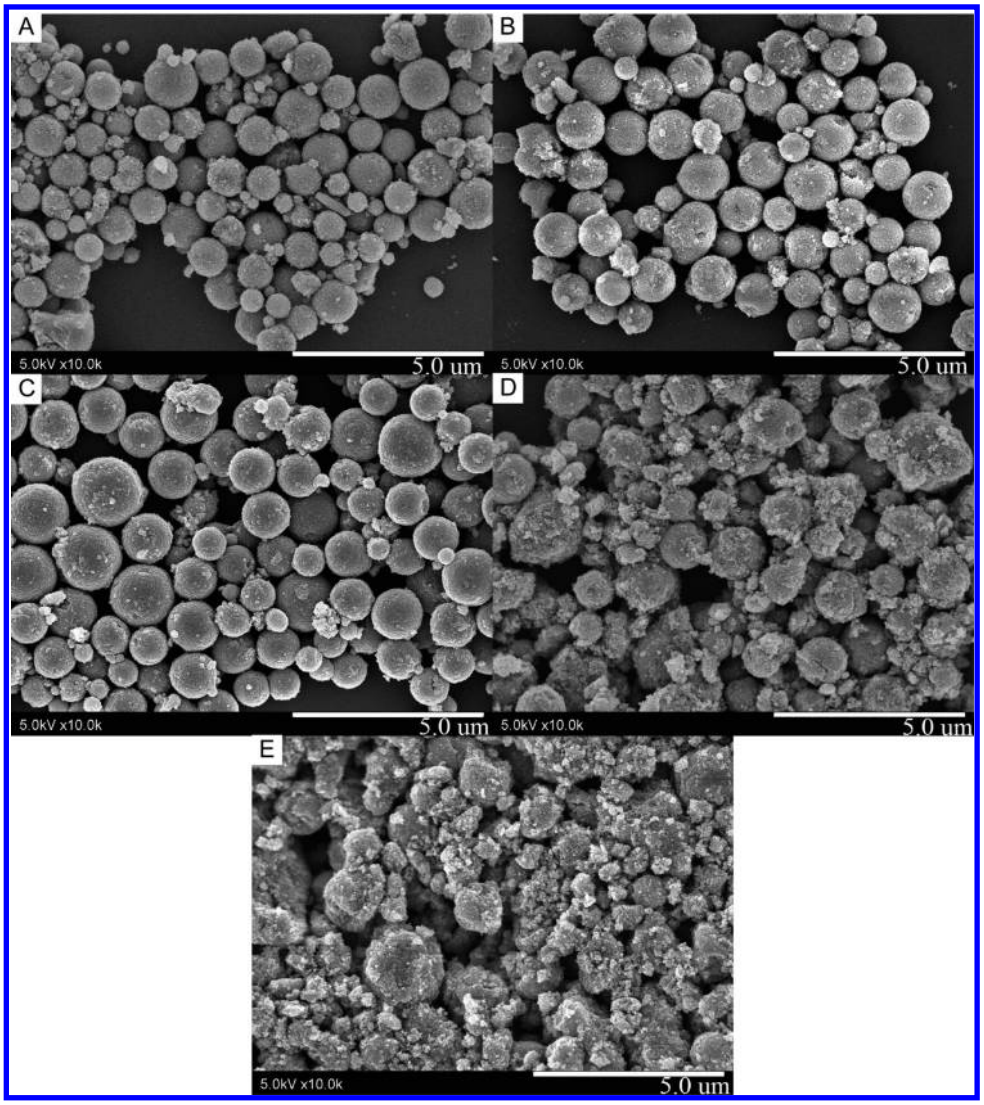

Figure 8. FE-SEM images of the mesoporous TiO_2 spheres obtained after hydrothermal treatment with different amounts of PVP being used during the electrospray process (A: 0.1 g of PVP; B: 0.2 g of PVP; C: 0.3 g of PVP; D: 0.4 g of PVP; E: 0.5 g of PVP).

that this sample has a bimodal pore size distribution and high pore volume. When 2.0 mL of acetic acid was added during hydrothermal treatment (Figure 3B), the number of larger pores decreases, suggesting that acetic acid causes the spheres to shrink. Spheres with a core−shell structure were also observed by FE-SEM, as shown in Figure 3C.

The FE-SEM images show that the TiO_2 spheres are composed of a large amount of interconnected nanoparticles. To ascertain the features of these nanoparticles, TEM was used to study the crystal morphology and facets. Parts A and B of Figure 4 show high-magnification TEM images of the nanoparticles in the TiO_2 spheres after hydrothermal treatment without and with 2.0 mL of acetic acid, respectively. The TiO_2 nanocrystals are around 10 nm in diameter and tend to form a truncated rhombic morphology. The nanocrystals have three sets of lattice fringes, which give three interplanar distances consistent with the (101), (−101), and (002) facets of the anatase phase, indicating that each rhombic single crystal lies in the (010) plane. A diagram of this rhombic crystal is shown in Figure 4C. The interior angles agree with the angle between the (101) and (−101) planes.[45]

The nanocrystals in the TiO_2 spheres have two exposed high energy facets: {001} and {010}. Because the formation of rhombic crystals is not perfect, interesting step-like {001} facets are observed, as highlighted in Figure 4A,B. These steps in the [001] (*c* axis) direction are caused by one- or two-dimensional defects, so their presence will increase the energy of the {001} surface, as well as its chemical reactivity. The percentage of exposed {001} facets decreases when 2.0 mL of acetic acid is added during hydrothermal treatment (Figure 4B). According to Xia et al.,[46] PVP molecules prefer to cap the {101} facets of anatase TiO_2 at low pH, so the presence of acetic acid will cause the nanocrystals grow in the [001] direction, resulting in the percentage of {001} surface decreasing.

X-ray diffraction (XRD) patterns of the TiO_2 spheres after hydrothermal treatment are presented in Figure 5. The TiO_2 spheres are composed of the anatase phase. The crystallinity improves as the content of acetic acid is increased. Applying the Scherrer equation to the (101) peaks,[47] the average size of the nanocrystals (average crystal length in the [101] direction) in the spheres is 7.7, 7.9, 8.3, and 10.1 nm when the amount of acetic acid

dx.doi.org/10.1021/la201547g |*Langmuir* 2011, 27, 8500–8508

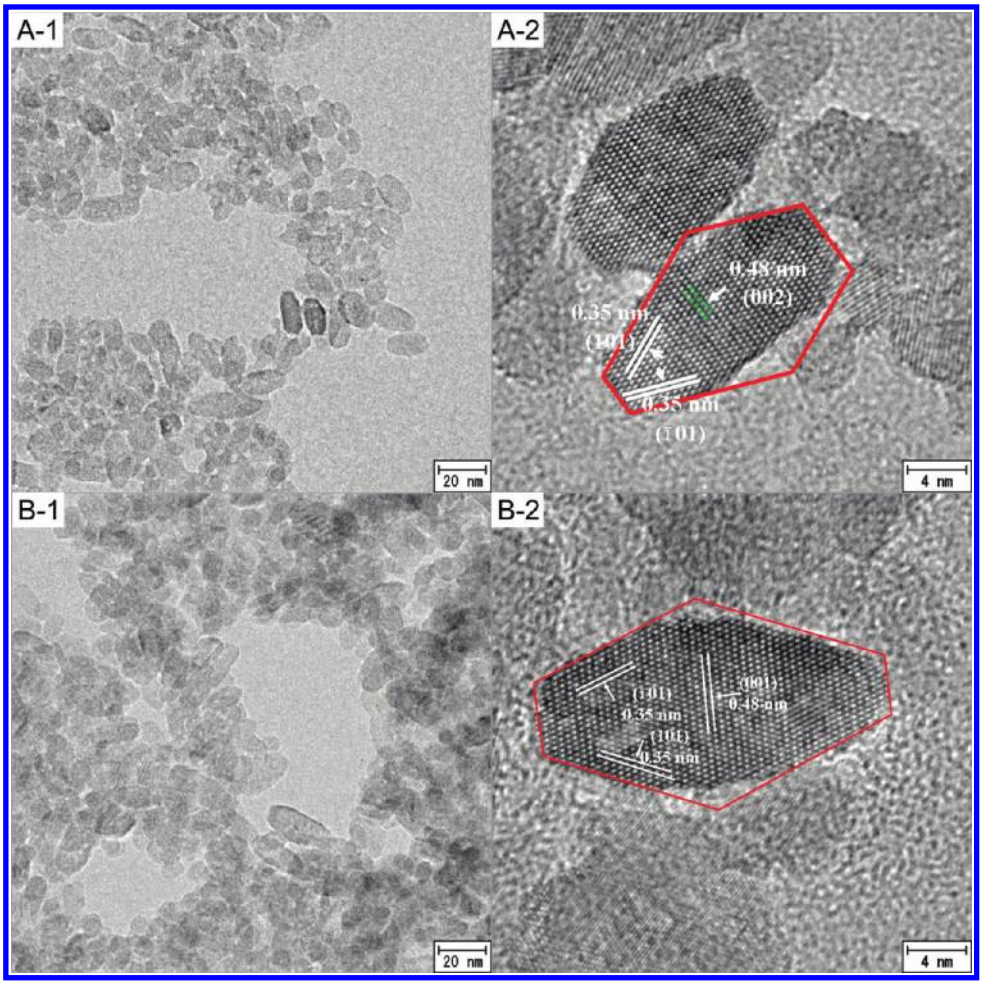

Figure 9. TEM images of the samples obtained after hydrothermal treatment with (A) 0.6 g and (B) 0.7 g of PVP being used in the electrospray process.

Table 4. Physical Properties of Mesoporous TiO_2 Spheres Containing Different Amounts of PVP

amount of PVP (g)	S_{BET} (m^2 g^{-1})	V_p (cm^3 g^{-1})	D_p (nm)	P (%)	d_{101} [a] (nm)	$d_{(001)}$ [b] (nm)	$d_{(001)}/d_{(101)}$
0.1	146	0.36	12	58	9.2	8.3	0.90
0.2	140	0.36	14	58	9.6	9.7	1.01
0.3	135	0.36	15.4	58	10.1	11.8	1.17
0.4	128	0.35	14	57	10.5	12.9	1.23
0.5	112	0.35	14	57	11.2	14.2	1.27
0.6					12.0	15.8	1.32
0.7					11.3	15.1	1.34

[a] Crystallite size calculated by applying Scherrer equation to the (101) peaks. [b] Crystallite size calculated by applying Scherrer equation to the (004) peaks.

added was 0, 0.5, 1.0, and 2.0 mL, respectively. Similarly, the crystal length in the [001] direction is 6.6, 8.5, 9.3, and 11.8 nm for 0, 0.5, 1.0, and 2.0 mL of acetic acid, respectively, when the Scherrer equation is applied to the (004) peaks. This shows that the percentage of exposed {001} facets decreases as the concentration of acetic acid increases, in accordance with the TEM analysis. The thickness of the crystals in the [010] direction was estimated using the formula $L(010) = 0.364L(211)$, where $L(010)$ is the crystal size in the [010] direction and $L(211)$ is the crystal size obtained from the (211) diffraction peak.[48] The thickness of the crystals in the TiO_2 spheres after hydrothermal post-treatment with 2.0 mL of acetic acid is ca. 4.8 nm, which is smaller than the lengths of the crystals in the [001] and [101] directions, indicating that they possess a nanosheet-like morphology.

Accurate data for the specific surface area, pore size, and pore volume of the nanospheres produced under different conditions are summarized in Table 2. The sample after hydrothermal treatment without acetic acid possesses a specific surface area and pore volume as high as 198 m^2 g^{-1} and 0.67 cm^3 g^{-1}, respectively. If acetic acid is used during hydrothermal treatment, both the specific surface area and pore volume decrease because the spheres shrink. As shown in Figure 6, without acetic acid, a

dx.doi.org/10.1021/la201547g |*Langmuir* 2011, 27, 8500–8508

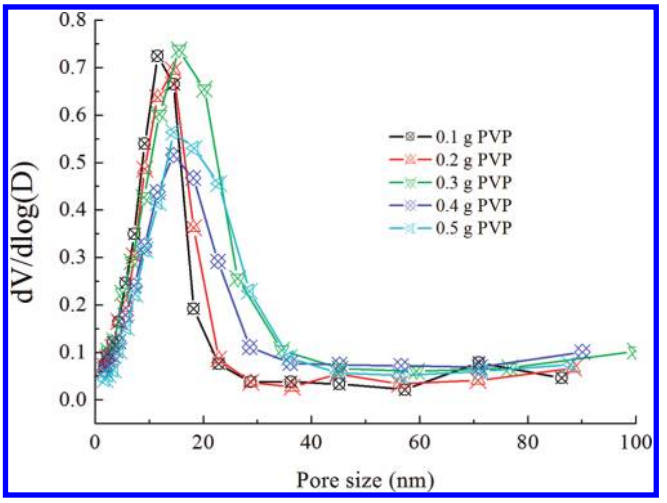

Figure 10. Pore size distributions of the mesoporous TiO_2 spheres obtained after hydrothermal treatment with different amount of PVP being used during the electrospray process.

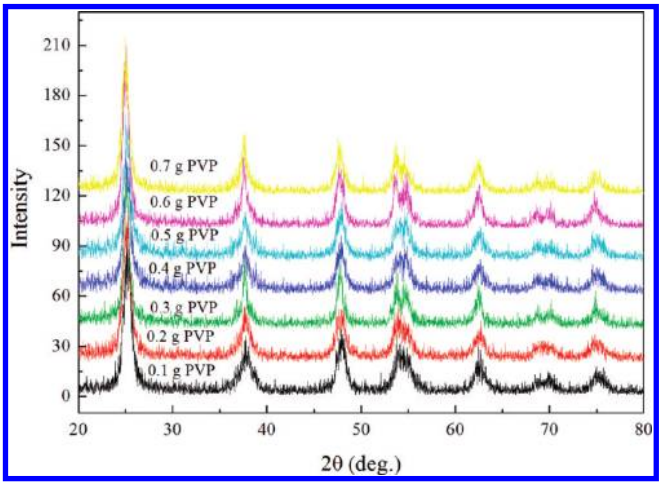

Figure 11. XRD patterns of mesoporous TiO_2 spheres obtained after hydrothermal treatment with different amounts of PVP used during the electrospray process.

bimodal pore size distribution is observed, which changes to a unimodal distribution after addition of acetic acid. The BET results confirm that the electrosprayed TiO_2 spheres transform into mesoporous structures with high surface area and high pore volume after hydrothermal treatment. Combining the above analyses, it is found that mesoporous TiO_2 spheres with a core−shell structure are successfully prepared. As well as high specific surface areas (>100 $m^2\ g^{-1}$) and high pore volumes (>0.30 $cm^{-3}\ g^{-1}$), interestingly, the TiO_2 spheres are composed of very small nanocrystals with exposed step-like {001} and {010} facets.

Effect of Hydrothermal Treatment Time on the Mesoporous Structure. To investigate the dynamic formation of mesoporous TiO_2 spheres during hydrothermal treatment, the effect of treatment time on the mesoporous TiO_2 spheres was studied. The specific surface area, pore volume, pore size, and pore percentage of the samples after hydrothermal treatment for different periods are summarized in Table 3. As shown in the above sections, the electrosprayed TiO_2 spheres have cores that

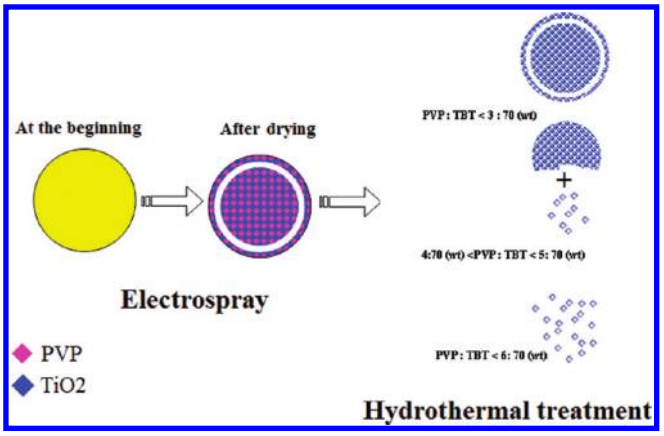

Figure 12. Diagram of the proposed formation mechanism of mesoporous TiO_2 core−shell spheres by electrospray and hydrothermal post-treatment.

contain pores with an average diameter of 60 nm. Compared with the initial electrosprayed particles, the specific surface area of the sample obtained after hydrothermal treatment for 5 h increases from 60 to 188 $m^2\ g^{-1}$, the pore size decreases from 60 to 12 nm, and the pore volume decreases from 0.54 to 0.40 $cm^3\ g^{-1}$. These results indicate that the spheres shrink during hydrothermal treatment because of the transformation of amorphous TiO_2 to the anatase phase. Further increasing the hydrothermal treatment period to 10, 20, and 24 h causes the specific surface area and pore volume to decrease correspondingly. However, the pore size increases slightly from 12 to 15 nm. Figure 7 shows the pore size distribution of the TiO_2 spheres after hydrothermal treatment for different periods. All of the samples obtained after hydrothermal treatment possess narrow pore size distributions at around 12−15 nm. The above analysis shows that the electrosprayed sample is not mesoporous, so the mesoporous structure forms during the course of hydrothermal treatment.

Effect of the Ratio of PVP:$Ti(OBu)_4$ on the Structure of TiO_2 Spheres. To study the mechanism of formation of mesoporous TiO_2 spheres, different samples were prepared by varying the content of PVP from 0.1 to 0.7 g and using the same contents of $Ti(OBu)_4$, ethanol, and acetic acid. FE-SEM images of the TiO_2 spheres obtained after 24 h hydrothermal treatment are presented in Figure 8. Before hydrothermal treatment, the morphology of the samples was checked by SEM, which confirmed that all of the samples have a spherical shape. It was found that hydrothermal treatment had a different effect on the morphology of the electrosprayed samples containing different amounts of PVP. The samples retain their spherical shape after hydrothermal treatment if the amount of PVP was less than 0.3 g. However, they start to disintegrate into tiny particles when more than 0.4 g of PVP was used. As shown in parts C and D of Figure 8, the samples obtained after hydrothermal treatment are composed of broken TiO_2 spheres and small nanoparticles when 0.4 and 0.5 g of PVP are used, respectively. Further increases in the amount of PVP leads to complete disintegration of the TiO_2 spheres. TEM images of the TiO_2 samples obtained after hydrothermal treatment when 0.6 and 0.7 g of PVP were used during electrospray are shown in Figure 9. Similar to Figure 3, the small TiO_2 nanocrystals possess imperfect rhombic shapes. High-resolution TEM images show that the nanoparticles have three sets of crystal fringes that correspond to the (101), (−101), and (001) facets of anatase TiO_2. These

dx.doi.org/10.1021/la201547g |*Langmuir* 2011, 27, 8500–8508

nanoparticles also contain two exposed step-like {001} and {010} facets.

The specific surface area, pore volume, pore size, percentage of pores, and crystal sizes of the TiO_2 spheres are presented in Table 4. The specific surface area decreases as the amount of PVP increases, while the pore volume and pore size remain almost unchanged. The pore size distributions of the samples obtained after hydrothermal treatment when different amounts of PVP were used during electrospray are shown in Figure 10. All of the samples have narrow pore size distributions, which increase in width slightly as the amount of PVP increases. The XRD patterns shown in Figure 11 reveal that the mesoporous TiO_2 spheres are mainly composed of the anatase phase. The average crystal lengths in the [101] and [001] directions are also shown in Table 4. The crystal size increases slightly as the content of PVP increases. Interestingly, the $d_{[001]}/d_{[101]}$ ratio also increases, indicating that the percentage of exposed {101} facets decreases as the amount of PVP increases, because more PVP molecules can cap the (101) surface of the nanocrystals when the amount of PVP is larger.

Proposed Formation Mechanism of TiO_2 Spheres. From the above observations of the TiO_2 spheres, it is proposed that their mechanism of formation is as follows. First, the PVP−TBT sol is atomized into a large number of microsized particles under high voltage during electrospray, which adopt spherical morphologies because of the surface tension across the particle surface. The spherical particles are highly dispersed in the air atmosphere, so the rapid vaporization of organic solvents and hydrolysis of titanium precursor (TBT) produces a solid surface on the TiO_2 spheres. This solid surface forms a protective layer that hinders further rapid vaporization and hydrolysis, so the complete hydrolysis of TiO_2 spheres takes several hours. The resulting slow vaporization and hydrolysis of the inside of the TiO_2 spheres will cause the inner spheres to shrink and collapse, resulting in a core−shell structure. This process is evidenced by the different structures of the shell and core, as seen in the SEM images (Figure 1A-2).

The PVP polymer forms a network during electrospray, and the amorphous TiO_2 particles fill the pores in this network. When the amount of PVP is large, the TiO_2 particles are separated into individual particles in the PVP network. Because the polymer network is destroyed during hydrothermal treatment, only tiny TiO_2 particles remain, as observed in FE-SEM (Figure 8) and TEM (Figure 9) images. At a low content of PVP, the amorphous TiO_2 can form a network within the PVP polymer network. Only the TiO_2 network remains after the PVP network is removed during hydrothermal treatment. In the present research, perfect mesoporous TiO_2 spheres are obtained if the PVP:TBT ratio is less than 3:70; individual tiny TiO_2 nanoparticles are obtained if the PVP:TBT ratio is more than 6:70; and a composite of nanoparticles and broken spheres is obtained when the PVP:TBT ratio is between 4:70 and 5:70. The formation of mesoporous TiO_2 spheres with core−shell structure derived from the above analysis is shown in Figure 12.

CONCLUSIONS

Interesting mesoporous core−shell TiO_2 spheres with high specific surface areas, high pore volumes, and narrow pore size distribution were prepared by a facile new method that combines electrospray and hydrothermal treatment. Spheres composed of small anatase TiO_2 nanocrystals with exposed high-energy facets, including step-like {001} and smooth {010} facets. The percentage of exposed {001} facets can be adjusted by changing the amount of PVP used during the electrospray process and the concentration of acetic acid added during hydrothermal treatment. The PVP:TBT ratio was found to be important to produce mesoporous TiO_2 spheres. It is proposed that the formation of an amorphous TiO_2 network within the electrosprayed TiO_2 spheres is crucial to obtaining mesoporous TiO_2 spheres. The high specific surface area, high pore volume, suitable pore size, spherical core−shell structure, and exposed high energy facets of these materials makes them attractive candidates for application in photocatalysis and DSSCs.

AUTHOR INFORMATION

Corresponding Author

*E-mail: pg-nakata@newkast.or.jp (K.N.); president@admin.tus.ac.jp (A.F.).

ACKNOWLEDGMENT

B. Liu acknowledges the Japan Society for the Promotion of Science (JSPS) for a Postdoctoral Fellowship for Foreign Researchers. K. Nakata and A. Fujishima acknowledge JSPS for financial support from the "Funding Program for World-Leading Innovative R&D on Science and Technology (FIRST Program)".

REFERENCES

(1) Tang, J.; Wu, Y.; McFarland, E. W.; Stucky, G. D. Synthesis and Photocatalytic Properties of Highly Crystalline and Ordered Mesoporous TiO_2 Thin Films. *Chem. Commun.* **2004**, 1670–1671.

(2) Ho, W.; Yu, J. C.; Lee, S. Synthesis of Hierarchical Nanoporous F-doped TiO_2 Spheres With Visible Light Photocatalytic Activity. *Chem. Commun.* **2006**, 1115–1117.

(3) Xiong, Z.; Dou, H.; Pan, J.; Ma, J.; Xu, C.; Zhao, X. S. Synthesis of Mesoporous Anatase TiO_2 With a Combined Template Method and Photocatalysis. *Cryst. Eng. Commun.* **2010**, *12*, 3455–3457.

(4) Hou, K.; Tian, B.; Li, F.; Bian, Z.; Zhao, D.; Huang, C. Highly Crystallized Mesoporous TiO_2 Films and Their Applications in Dye-Sensitized Solar Cells. *J. Mater. Chem.* **2005**, *15*, 2414–2420.

(5) Ahn, S. H.; Koh, J. H.; Seo, J. A.; Kim, J. H. Structure Control of Organized Mesoporous TiO_2 Films Templated by Graft Copolymers for Dye-sensitized Solar Cells. *Chem. Commun.* **2010**, *46*, 1935–1937.

(6) Yang, W.; Wan, F.; Chen, Q.; Li, J.; Xu, D. Controlling Synthesis of Well-Crystallized Mesoporous TiO_2 Microspheres With Ultrahigh Surface Area for High-Performance Dye-Sensitized Solar Cells. *J. Mater. Chem.* **2010**, *20*, 2870–2876.

(7) Ding, S.; Chen, J.; Wang, Z.; Cheah, Y.; Madhavi, S.; Hu, X.; Lou, X. TiO_2 Hollow Spheres With Large Amount of Exposed (001) Facets for Fast Reversible Lithium Storage. *J. Mater. Chem.* **2011**, *21*, 1677–1680.

(8) Seifert, J. M.; Feckl, J. M.; Fattakhova-Rohlfing, D.; Liu, Y.; Kalousek, V.; Rathousky, J.; Bein, T. Ultrasmall Titania Nanocrystals and Their Direct Assembly Into Mesoporous Structures Showing Fast Lithium Insertion. *J. Am. Chem. Soc.* **2010**, *132*, 12605–12611.

(9) Periyat, P.; Leyland, N.; McCormack, D. E.; Colreavy, J.; Corr, D.; Pillai, S. C. Rapid Microwave Synthesis of Mesoporous TiO_2 for Electrochromic Displays. *J. Mater. Chem.* **2010**, *20*, 3650–3655.

(10) Zhang, Y.; Xie, Z.; Wang, J. Supramolecular-Templated Thick Mesoporous Titania Films for Dye-Sensitized Solar Cells: Effect of Morphology on Performance. *ACS Appl. Mater. Interfaces* **2009**, *1*, 2789–2795.

(11) Lei, B.; Liao, J.; Zhang, R.; Wang, J.; Su, C.; Kuang, D. Ordered Crystalline TiO_2 Nanotube Arrays on Transparent FTO Glass for Efficient Dye-Sensitized Solar Cells. *J. Phys. Chem. C* **2010**, *114*, 15228–15233.

(12) Shang, M.; Wang, W.; Zhang, L.; Sun, S.; Wang, L.; Zhou, L. 3D Bi_2WO_6/TiO_2 Hierarchical Heterostructure: Controllable Synthesis and Enhanced Visible Photocatalytic Degradation Performances. *J. Phys. Chem. C* **2009**, *113*, 14727–14731.

(13) Ye, J.; Liu, W.; Cai, J.; Chen, S.; Zhao, X.; Zhou, H.; Qi, L. Nanoporous Anatase TiO_2 Mesocrystals: Additive-Free Synthesis, Remarkable Crystalline-Phase Stability, and Improved Lithium Insertion Behavior. *J. Am. Chem. Soc.* **2011**, *133*, 933–940.

(14) Zhong, L.; Hu, J.; Wan, L.; Song, W. Facile Synthesis of Nanoporous Anatase Spheres and Their Environmental Applications. *Chem. Commun.* **2008**, 1184–1186.

(15) Chen., D.; Cao, L.; Huang, F.; Imperia, P.; Cheng, Y.; Caruso, R. A. Synthesis of Monodisperse Mesoporous Titanium Beads with Controllable Diameters, High Surface Area, and Variable Pore Diameters. *J. Am. Chem. Soc.* **2010**, *132*, 4438–4444.

(16) Huang, F.; Chen, D.; Zhang, X.; Caruso, R. A.; Cheng, Y. Dual-Function Scattering Layer of Submicrometer-Sized Mesoporous TiO_2 Beads for High Efficiency Dye-Sensitized Solar Cells. *Adv. Funct. Mater.* **2010**, *20*, 1301–1305.

(17) Chen, D.; Huang, F.; Cheng, Y.; Caruso, R. A. Mesoporous Anatase TiO_2 Beads With High Surface Areas and Controllable Pore Sizes: a Superior Candidate for High-Performance Dye-Sensitized Solar Cells. *Adv. Mater.* **2009**, *21*, 2206–2210.

(18) Bazilevsky, A. V.; Yarin, A. L.; Megaridis, C. M. Co-electrospinning of Core-Shell Fibers Using a Single-Nozzle Technique. *Langmuir* **2007**, *23*, 2311–2314.

(19) Li, D.; Xia, Y. Direct Fabrication of Composite and Ceramic Hollow Nanofibers by Electrospinning. *Nano Lett.* **2004**, *4*, 933–938.

(20) Li, H.; Bian, Z.; Zhu, J.; Zhang, D.; Li, G.; Huo, Y.; Li, H.; Lu, Y. Mesoporous Titania Spheres with Tunable Chamber Structure and Enhanced Photocatalytic Activity. *J. Am. Chem. Soc.* **2007**, *129*, 8406–8407.

(21) Sauvage, F.; Chen, D.; Comete, P.; Huang, F.; Heiniger, L.; Cheng, Y.; Caruso, R. A.; Craetzel, M. Dye-Sensitized Solar Cells Employing a Single Film of Mesoporous TiO_2 Beads Achieve Power Conversion Efficiencies Over 10%. *ACS Nano* **2010**, *4*, 4420–4425.

(22) Han, X.; Kuang, Q.; Jin, M.; Xie, Z.; Zheng, L. Synthesis of Titania Nanosheets with a High percentage of Exposed (001) Facets and Related Photocatalytic Activities. *J. Am. Chem. Soc.* **2009**, *131*, 3152–3153.

(23) Zhang, D.; Li, G.; Yang, X.; Yu, J. C. A Micrometer-sized TiO_2 Single-Crystal Photocatalyst With Remarkable 80% Level of Reactive Facets. *Chem. Commun.* **2009**, 4381–4383.

(24) Zhu, J.; Wang, S.; Bian, Z.; Xie, S.; Cai, C.; Wang, J.; Yang, H.; Li, H. Solvothermally Controllable Synthesis of Anatase TiO_2 Nanocrystals With Dominant {001} Facets and Enhanced Photocatalytic Activity. *Cryst. Eng. Commun.* **2010**, *12*, 2219–2224.

(25) Yang, X.; Li, Z.; Liu, G.; Xing, J.; Sun, C.; Yang, H.; Li, C. Ultrathin anatase TiO_2 nanosheets dominated with {001} facets: thickness-controlled synthesis, growth mechanism and water-splitting properties. *Cryst. Eng. Commun.* **2011**, *13*, 1378–1383.

(26) Rathouský, J.; Kalousek, V.; Kolář, M.; Jirkovský, A. Mesoporous Films of TiO_2 as Efficient Photocatalysts for the Purification of Water. *Photochem. Photobiol. Sci.* **2011**, *10*, 419–424.

(27) Liu, X.; Geng, D.; Wang, X.; Ma, S.; Wang, H.; Li, D.; Li, B.; Liu, W.; Zhang, Z. Enhanced Photocatalytic Activity of Mo−{001}TiO_2 Core−Shell Nanoparticles Under Visible Light. *Chem. Commun.* **2010**, *46*, 6956–6958.

(28) Liu, M.; Piao, L.; Zhao, L.; Ju, S.; Yan, Z.; He, T.; Zhou, C.; Wang, W. Anatase TiO_2 Single Crystals With Exposed {001} and {110} Facets: Facile Synthesis and Enhanced Photocatalysis. *Chem. Commun.* **2010**, *46*, 1664–1666.

(29) Liu, G.; Sun, C.; Yang, H.; Smith, S. C.; Wang, L.; Lu, G.; Cheng, H. Nanosized Anatase TiO_2 Single Crystals for Enhanced Photocatalytic Activity. *Chem. Commun.* **2010**, *46*, 755–757.

(30) Ma, X.; Chen, Z.; Hartono, S. B.; Jiang, H.; Zou, J.; Qiao, S.; Yang, H. Fabrication of Uniform Anatase TiO_2 Particles Exposed by {001} Facets. *Chem. Commun* **2010**, *46*, 6608–6610.

(31) Yu, J.; Fan, J.; Lv, K. Anatase TiO_2 Nanosheets With Exposed (001) Facets: Improved Photoelectric Conversion Efficiency in Dye-Sensitized Solar Cells. *Nanoscale* **2010**, *2*, 2144–2149.

(32) Wang, X.; Liu, G.; Wang, L.; Pan, J.; Lu, G.; Cheng, H. TiO_2 Films With Oriented Anatase {001} Facets and Their Photoelectrochemical Behavior as CdS Nanoparticle Sensitized Photoanodes. *J. Mater. Chem.* **2011**, *21*, 869–873.

(33) Chen, J.; Tan, T.; Li, C.; Cheah, L.; Luan, D.; Madhavi, S.; Boey, F. Y. C.; Archer, L. A.; Lou, X. Constructing Hierarchical Spheres From Large Ultrathin Anatase Nanosheets With Nearly 100% (001) Facets for Fast Reversible Lithium Storage. *J. Am. Chem. Soc.* **2010**, *132*, 6124–6130.

(34) Wu, B.; Guo, C.; Zheng, N.; Xie, Z.; Stucky, G. D. Nonaqueous Production of Nanostructured Anatase with High Energy Facets. *J. Am. Chem. Soc.* **2008**, *130*, 17563–17567.

(35) Yu, J.; Xiang, Q.; Ran, J.; Mann, S. One-step Hydrothermal Fabrication and Photocatalytic Activity of Surface-Fluorinated TiO_2 Hollow Microspheres and Tabular Anatase Single Microcrystals With High-Energy Facets. *Cryst. Eng. Commun.* **2010**, *12*, 872–879.

(36) Liu, S.; Yu, J.; Jaroniec, M. Tunable Photocatalytic Selectivity of Hollow TiO_2 Microspheres Composed of Anatase Polyhedra With Exposed {101} Facets. *J. Am. Chem. Soc.* **2010**, *132*, 11914–11916.

(37) Dinh, C.; Nguyen, T.; Kleitz, F.; Do, T. Shape-Controlled Synthesis of Highly Crystalline Titania Nanocrystals. *ACS Nano* **2009**, *3*, 3737–3743.

(38) Nam, S. H.; Shim, H.-S.; Kim, Y.-S.; Dar, M. A.; Kim, J. G.; Kim, W. B. Ag or Au Nanoparticle-Embedded One-Dimensional Composite TiO_2 Nanofibers Prepared via Electrospinning for Use in Lithium-Ion Batteries. *ACS Appl. Mater. Interfaces* **2010**, *2*, 2046–2052.

(39) Formo, E.; Lee, E.; Campbell, D.; Xia, Y. Functionalization of Electrospun TiO_2 Nanofibers with Pt Nanoparticles and Nanowires for Catalytic Applications. *Nano Lett.* **2008**, *8*, 668–672.

(40) Chen, H.; Zhao, Y.; Song, Y.; Jiang, L. One-step Multicomponent Encapsulation by Compound-Fluidic Electrospray. *J. Am. Chem. Soc.* **2008**, *130*, 7800–7801.

(41) Zhao, T.; Liu, Z.; Nakata, K.; Nishimoto, S.; Murakami, T.; Zhao, Y.; Jiang, L.; Fujishima, A. Multichannel TiO_2 Hollow Fibers With Enhanced Photocatalytic Activity. *J. Mater. Chem.* **2010**, *20*, 5095–5099.

(42) Zhao, Y.; Cao, X.; Jiang, L. Bio-mimic Multichannel Microtubes by a Facile method. *J. Am. Chem. Soc.* **2007**, *129*, 764–765.

(43) Roh, K.-H.; Martin, D. C.; Lahann, J. Triphasic Nanocolloids. *J. Am. Chem. Soc.* **2006**, *128*, 6796–6797.

(44) Loscertales, I. G.; Barrero, A.; Guerrero, I.; Cortijo, R.; Marquez, M.; Gañán-calvo, A. M. Micro/Nano Encapsulation via Electrified Coaxial Liquid Jets. *Science* **2002**, *295*, 1695–1698.

(45) Wang, D.; Liu, J.; Huo, Q.; Nie, Z.; Lu, W.; Williford, R. E.; Jiang, Y. Surface-Mediated Growth of Transparent, Oriented, and Well-Defined Nanocrystalline Anatase Titania Films. *J. Am. Chem. Soc.* **2006**, *128*, 13670–13671.

(46) Dai, Y.; Cobley, C. M.; Zeng, J.; Sun, Y.; Xia, Y. Synthesis of Anatase TiO_2 Crystals With Exposed {001} Facets. *Nano Lett.* **2009**, *9*, 2455–2459.

(47) Wang, B. X.; Cai, G.; Wen, L.; Song, Y.; Zhao, X. Low Temperature Fabrication of V-doped TiO_2 Nanoparticles: Structure and Photocatalytic Studies. *J. Hazard. Mater.* **2009**, *169*, 1112–1118.

(48) Howard, C. J.; Sabine, T. M.; Dickson, F. Structural and thermal parameters for rutile and anatase. *Acta Crystallogr., Sect. B* **1991**, *47*, 462–468.